Icarus **153**, 130–147 (2001)
doi:10.1006/icar.2001.6659, available online at http://www.idealibrary.com on IDEAL®

Three-Dimensional Modeling of the Tropospheric Methane Cycle on Titan

Tetsuya Tokano, Fritz M. Neubauer, and Manfred Laube

Institut für Geophysik und Meteorologie, Universität zu Köln, Albertus-Magnus-Platz, 50923 Köln, Germany
E-mail: tetsuya.tokano@dlr.de

and

Christopher P. McKay

Space Science Division, NASA Ames Research Center, Moffett Field, California 94035-1000

Received August 28, 2000; revised May 3, 2001

The tropospheric methane cycle on Titan including advection, diffusion, condensation, precipitation, evaporation, and surface source is simulated by a three-dimensional general circulation model. The model takes into account the different nucleation of methane in Titan's troposphere, and assumes condensation whenever the saturation ratio (relative humidity) exceeds a critical value of either 100 or 150%. The simulation with the latter critical saturation is shown to be more compatible with the *Voyager* data. The meridional circulation accounts for a seasonal methane transport from the winter to summer hemisphere in the mid-troposphere, causing a higher supersaturation in late summer and early autumn. Condensation preferentially occurs in this season at 15 km altitude at low latitudes. The occasional character may be explained by the high critical saturation ratio, which cannot be often exceeded. Falling rain evaporates during the descent, so no rain arrives at the surface. The hydrological cycle of methane on Titan takes place mostly within the atmosphere. The latitudinal methane distribution near the surface cannot be reproduced by transport, evaporation, condensation, and combinations of them, indicating some undetermined surface processes affecting the methane distribution. The zonal and meridional circulation is sensitive to the methane distribution.

Key Words: **Titan; atmospheres; structure; meteorology.**

1. INTRODUCTION

Saturn's largest moon Titan resembles the Earth in that it possesses a dense atmosphere, which mainly consists of molecular nitrogen, but contains also a large amount of methane. The manyfold importance of methane to Titan's climate has attracted much attention in recent years. First, methane is one of the precursors of Titan's diverse photochemistry, which is ultimately responsible for the formation of various hydrocarbons, nitriles, and stratospheric aerosols. Secondly, methane significantly contributes to absorption of both solar near-infrared radiation and thermal radiation (greenhouse effect), controlling the thermal structure of Titan's atmosphere. Thirdly, the temperature, pressure, and methane abundance in Titan's troposphere are such that methane could be present in all three phases, i.e., phase changes as well as meteorological phenomena correlated with them could occur. The latter two effects are strongly suggestive of the role H_2O plays on Earth, whose distribution profoundly controls the weather and climate. Exact knowledge of the methane distribution is also important in the determination of the temperature from remote sensing data. The retrievement of the vertical temperature profile from the radio occultation data strongly depends on the molecular weight, which varies with the mole fractions of the gases. Furthermore, in retrieving the latitudinal temperature distribution in the upper stratosphere from the observed ν_4 methane bands, it was tacitly assumed that the methane distribution in the stratosphere would be uniform (Flasar *et al*. 1981, Flasar and Conrath 1990, Coustenis and Bézard 1995).

Despite this importance, little is known about the behavior of methane in the troposphere including condensation, transport, sources, and sinks. This is owing to the difficult measurements and observations of Titan's troposphere due to the dense stratospheric haze layer. The most certain assumption concerning Titan's atmospheric methane is that it should be supplied externally, perhaps from the surface, since there are no net sources within the atmosphere, but several sinks. Methane is irreversibly decomposed by photochemistry (27% by direct photolysis, 73% by catalytic cycles), and without having an external source, Titan's atmospheric methane would deplete within about 10^7 years (Yung *et al*. 1984). Lorenz *et al*. (1997) showed by means of the radiative–convective model of McKay *et al*. (1989) that Titan's atmosphere could at any time collapse episodically due to the condensation of nitrogen as a consequence of the diminished greenhouse effect and subsequent temperature drop if the methane supply stops for a long period. It is also suggested that a runaway greenhouse effect may be expected in the future if the total volatile inventory of Titan is large and the methane supply continues (Lorenz *et al*. 1999).

0019-1035/01 $35.00

On the other hand, the nonphotochemical fate of methane in the troposphere is also crucial in understanding Titan's atmosphere. As reviewed by McKay *et al*. (2001), there is no general concensus among researchers about condensation processes in Titan's troposphere. While *Voyager* infrared spectra seem to indicate high methane supersaturation in some parts of Titan's troposphere (Courtin *et al*. 1995, Samuelson *et al*. 1997), there are also suggestions of spectroscopic identifications of tropospheric clouds (Griffith *et al*. 1998, 2000). Methane condensation on Titan is generally thought to be difficult due to the low temperature and supposed lack of suitable condensation nuclei. Currently, there are several studies treating Titan's methane condensation in one-dimensional models (Toon *et al*. 1988, Courtin *et al*. 1995, Samuelson and Mayo 1997; Guez *et al*. 1997, McKay *et al*. 1997), but in all models the vertical eddy diffusion is the only transport mode considered, while advective transports in both horizontal and vertical directions are totally ignored. Atmospheric general circulation models (GCMs) for Titan indicate that Hadley-type meridional circulation may be expected (Hourdin *et al*. 1995, Tokano *et al*. 1999), which may be important for the global transport of atmospheric constituents.

In this paper we perform a model simulation of Titan's atmospheric methane cycle by a GCM, taking into account transport and condensation processes. A GCM is a three-dimensional numerical climate model based on basic equations of hydrodynamics, which describe the conservation of mass, energy, and momentum as well as the state of the atmosphere. These equations are solved to predict the time evolution of meteorological variables in a global frame.

The work addresses the following questions:

1. How does the global atmospheric circulation affect the methane distribution and vice versa?
2. What is the atmospheric condition favoring methane condensation on Titan? Where and when may clouds be expected?
3. How is the global distribution and amount of precipitation controlled?
4. How is the climate affected by the variability of the atmospheric methane abundance?

In Section 2 we review what is currently known or speculated about Titan's tropospheric methane and in Sections 3 and 4 we present our model study. Section 5 discusses the results.

2. OBSERVATION, THEORY, AND MODELING

Methane in Titan's atmosphere was discovered by Kuiper (1944) as Titan's first gas species, earlier than the discovery of methane in the terrestrial atmosphere by Migeotte (1948). Nevertheless, the knowledge of its abundance on Titan is still restricted.

By means of CCD spectrophotometry, Karkoschka (1998) determined the mean methane pathlength in Titan's atmosphere to 4 km-am, providing a constraint on the column methane abundance. The spatial distribution of methane in the troposphere is constrained to some extent by the *Voyager 1* data as well as some general assumptions about the fate of methane. The source of methane in Titan's atmosphere is assumed to be located at the surface since neither photochemistry nor gas-phase chemistry provides net production of methane. This led initially to the idea of a global ethane–methane ocean (Flasar 1983, Lunine et al. 1983), which has recently been ruled out due to inconsistencies with surface observations. Methane sources are assumed at the surface, though, e.g., in the form of evaporation from isolated hydrocarbon lakes (McKay *et al*. 1993), diffusion from a subsurface ocean (Kossacki and Lorenz 1996, Fortes 2000), cryovolcanism (Lorenz 1996), or methane hydrate (Loveday *et al*. 2001). This assumption implies that the methane mole fraction is likely not to increase with altitude within the homosphere.

Earlier studies assumed that the tropospheric methane abundance should be exactly limited by saturation (e.g., Lellouch *et al*. 1989). The most important argument for this assumption is the fact that the observed IRIS spectrum shape at 200–600 cm^{-1} can only be fit if the methane mole fraction in the troposphere decreases substantially with altitude, which implies condensation and precipitation at some altitude. However, recent studies indicate that high supersaturation of gaseous methane is likely. Courtin *et al*. (1995) and Samuelson *et al*. (1997) independently performed an analysis of the IRIS spectra by comparing computed synthetic spectra with observed spectra, and found that strong supersaturation with saturation ratios up to 200 or 160%, respectively, in some part of the troposphere would be necessary in order to fit the spectra at long wavelengths (200–300 cm^{-1}). Samuelson *et al*. (1997) furthermore deduced the latitudinal distribution of the methane mole fraction immediately above the surface. It decreases from about 6% at the equator down to less than 2% at high latitudes. McKay *et al*. (1997) reanalyzed the radio occultation data, examining the change in temperature lapse rate considering various states of methane condensation. They concluded that the surface methane saturation ratio is limited to 60% if methane condensation is allowed since otherwise an unrealistically high superadiabatic lapse rate would be required in order to match the data, but it is not limited if high supersaturation of more than 140% is allowed.

Among several estimates two quite different vertical methane profiles constructed by Lellouch *et al*. (1989) and Yelle *et al*. (1997), respectively, are widely used. In the model of Lellouch *et al*. (1989) the methane mole fraction at the surface is 8%, corresponding to a relative humidity of 66%. It remains constant until saturation at 3 km, then decreases following the saturation curve until the minimum value of 1.5%, which is also the constant stratospheric value. The recent engineering model of Yelle *et al*. (1997) assumes a constant methane mole fraction of 3% in the entire troposphere and stratosphere, implying substantial supersaturation up to 140% in the mid-troposphere.

For a long time it was not clear whether substantial methane condensation is occurring in Titan's troposphere. The existence of liquid or solid methane as such on Titan has not been confirmed yet by observation. The global haze layer has always

inhibited direct observation of clouds, falling rain, or polar caps, which would be indicative of the occurrence of condensation. Toon *et al*. (1988) investigated by means of a radiative transfer model which type of methane clouds is compatible with observed IRIS spectra. They showed that patchy clouds with typical particle sizes of more than 50 μm and a particle number density of less than 10^{-3} cm^{-3} should be possible. For the first time, Griffith *et al*. (1998) reported on a possible detection of tropospheric clouds by telescopic observation. They observed the spectrum in the near-infrared methane window by the UKIRT (United Kingdom Infrared Telescope), and recognized an unusual increase of the geometric albedo at 2 μm in September 1995. After isolating albedo contributions from the surface, gas, and haze, this sudden increase could be ascribed to the reflection by a transient cloud cover located at about 15 km altitude near the equator, covering 9% of Titan's disk. Griffith *et al*. (2000) reported on further short-lived clouds in 1999.

The presence of clouds may indicate the occurrence of precipitation, too. Tropospheric condensates on Titan would not consist of pure methane, but of a mixture of nitrogen and methane (Thompson *et al*. 1992). Consequently, methane can exist in liquid phase down to 80.6 K (well below the triple point of pure methane, 90.68 K), and the saturation vapor pressure is 20% lower and the condensation heat 10% lower than that of pure methane. On the average condensed methane would be solid above 12 km altitude, and would melt below this level. Lorenz (1993) calculated by means of a simple microphysics model the characteristics of possible raindrops on Titan, and concluded that under Titan's tropospheric condition raindrops would be larger (up to 9.5 mm diameter), and have smaller fall velocities ($<$2 m s^{-1}) than terrestrial raindrops, and evaporate mostly before reaching the surface.

Samuelson and Mayo (1997) developed a steady-state methane condensation model in order to obtain the vertical distribution of methane mole fraction, raindrop size, and saturation ratio. In the model solid ethane particles precipitating down from the stratosphere are treated as condensation nuclei, and the loss of methane due to condensation and precipitation is exactly balanced by replacement of methane vapor by eddy diffusion. The result was strongly dependent on the initial ethane particle radii rather than on the methane abundance. In general, the larger the nucleus radii, the larger the supersaturation in the upper troposphere (and thus less precipitation), because less nucleation sites are available. They and Samuelson *et al*. (1997) speculated that the polar region around the vernal equinox may be the most favorable condition for methane condensation due to the enhanced downward ethane particle flux.

The high supersaturation or equivalently the difficult nucleation of methane under Titan conditions has been ascribed to the low temperature and lack of suitable condensation nuclei (Courtin *et al*. 1995, Guez *et al*. 1997). The first theoretical study of methane condensation in a real atmosphere by Moses *et al*. (1992) investigated the hydrocarbon nucleation in Neptune's atmosphere by an application of the classical nucleation theory described, e.g., in Pruppacher and Klett (1978). Much of it may also apply to Titan on which are found low temperatures similar to those on Neptune. Among the several nucleation mechanisms only the heterogeneous nucleation onto condensation nuclei was shown to be efficient enough at realistic methane saturation ratios, while homogeneous or ion-induced nucleation was not efficient enough to become important. They developed a concept of the critical saturation ratio (at which the nucleation rate exceeds 10^{-2} cm^{-3} s^{-1}), which substantially depends on the size of the condensation nuclei and the contact angle between the nuclei and condensate, according to the classical nucleation theory. The nucleation rate of methane is more sensitive to the saturation ratio than to contact angle (between the condensate and condensation nucleus) and radius of the nucleus. Significant nucleation rates are found while methane is in a small range of saturation ratios (critical saturation ratio) for all choices of nucleus radii and contact angles. They showed that for sufficiently small condensation nuclei and small contact angles noteable condensation can set in at saturation ratios below 200%. Courtin *et al*. (1995) and Guez *et al*. (1997), who applied the classical nucleation theory to Titan's methane clouds, suggested that in the case of Titan condensation may be inhibited.

3. SIMULATION OF METHANE CYCLE

3.1. Concept and Procedure of the Methane Cycle Simulation

The aim of this study is to model and analyze the fate of atmospheric methane and its feedback to Titan's climate by a GCM. Ideally the study of Titan's methane cycle should cover the atmospheric and "hydrological" branch and the coupling between them. The current study deals primarily with the atmospheric branch that most affects the climate directly.

A major advantage of this model is the ability to model the advective transport of methane vapor and couple the varying distribution to radiation. A possible spatial and temporal variation of the methane abundance is an important aspect not considered in earlier works. The three-dimensional structure of the GCM is valuable in that the large-scale atmospheric dynamics is self-consistently calculated by basic equations of hydrodynamics, so the precision of the advective methane transport does not suffer from approximations necessary in two-dimensional models.

In our GCM we consider the following processes that methane on Titan in gaseous, liquid, or solid phase may undergo, except for those which are written in *italic*:

- *Photochemical destruction*
- Transport: diffusion, advection
- Phase change: condensation, evaporation, latent heat exchange
- Transport in liquid/solid phase: precipitation, *rivers?*
- *Subgrid- and meso-scale processes*
- Greenhouse effect (collision-induced absorption)
- Sources, *interaction with the surface?*
- *Subsurface methane cycle?*

For this purpose an additional prognostic variable, the methane mole fraction C, is introduced in the GCM. The tendency (time derivative) of the methane mole fraction is written as

$$\frac{\partial(\rho C)}{\partial t} = -\nabla \cdot (\rho \mathbf{v} C) - \frac{\partial(\rho w C)}{\partial z} + \frac{1}{\rho}\frac{\partial}{\partial z}\left(K\frac{\partial(\rho C)}{\partial z}\right) \quad (1)$$

where ρ is the air density, $\mathbf{v}$ is the horizontal wind vector, w is the vertical wind, z is the altitude, and K is the eddy diffusion coefficient. The first and second terms on the right-hand side describe the horizontal and vertical advection, respectively, and the third term is the vertical eddy diffusion. In the model Eq. (1) is written in the form of a tendency equation for atmospheric constituents used in the GEOS (Goddard Earth-Observing System) GCM (Takacs *et al*. 1994, Suarez and Takacs 1995) on which our GCM is based. For the advection of methane the same finite-difference scheme is used as in other prognostic equations of the GCM.

An important aspect in this study is the condensation of methane. Condensation modeling in a GCM requires a cloud parameterization scheme that reproduces cloud characteristics representative of the entire area covered by a single gridpoint. In terrestrial GCMs convective and stratiform clouds are generally treated separately with cloud formation schemes developed for this purpose, bypassing sophisticated microphysics modeling that is impractical in GCMs. Convective clouds are parameterized in order to give a statistical description of the effect of a patchy and complex spectrum of subgrid-scale clouds on the mesh large-scale variables. On the other hand, the properties of Titan's clouds are poorly constrained and the type of observed clouds is far from being understood. In this peculiar situation the first approach should not be to adopt a cloud scheme developed for terrestrial H_2O clouds. Instead of this, it appears better first to simulate simple but extreme scenarios concerning methane condensation and infer from the results the more likely scenario and atmospheric condition favorable for cloud formation.

The treatment of condensation, evaporation, and rainout as well as the temperature change due to latent heat exchange is discussed in Section 3.3 and the scheme is described in the Appendix. The instantaneous global methane distribution is used in the calculation of the radiative fluxes. On the other hand, radiative effects of possible methane clouds are not taken into account because we generally assume that clouds are short-lived compared to the radiative time constant in Titan's troposphere.

3.2. General Circulation Model

The GCM we use in this paper is essentially the same as that of Tokano *et al*. (1999), so we give only a brief model description here. It is a three-dimensional hydrostatic general circulation model of Titan's lower atmosphere (troposphere and stratosphere) based on primitive equations. The radiation is calculated by the model of McKay *et al*. (1989), considering the absorption and scattering of solar radiation by stratospheric haze and methane, collision-induced absorption by the greenhouse gases N_2, CH_4, and H_2, and absorption by permitted transitions of C_2H_6 (ethane) and C_2H_2 (acetylene) in the stratosphere. The seasonal variation of insolation including Saturn's obliquity and eccentricity is accounted for. The ground temperature T_g is fixed to a prescribed value, which decreases from 95 K at the equator to 90 K at the poles. We have not accounted for a possible seasonal cycle of T_g because at the moment nothing is known about the thermal properties of Titan's surface. The GCM is a gridpoint model, and uses the numerical scheme ("dynamical core") of Aries/Geos GCM (Suarez and Takacs 1995) developed at the NASA Goddard Space Flight Center.

The following modifications to the GCM of Tokano *et al*. (1999) have been made for this study: the vertical grid resolution is doubled to 60 vertical layers, the vertical eddy diffusion coefficient K (for all prognostic variables) is decreased to 0.05 m^2 s^{-1}, the variation of stratospheric aerosols is not predicted, but the methane mole fraction is predicted. We use this smaller coefficient in order to keep the diffusive transport smaller than the advective transport.

3.3. Simulated scenarios

The simulation of different scenarios is necessary since we are not aware of the condensation processes and methane sources on Titan. However, a limitation of the study to a few representative cases is indispensable due to the huge computational requirement of the three-dimensional GCM. Two simplified but representative cases (scenarios) are simulated in this study.

Case 1. Condensation at saturation ratios exceeding 100%. Whenever a particular gridpoint becomes supersaturated, i.e., the saturation ratio (relative humidity) exceeds 100%, the excess fraction of gaseous methane is immediately converted to the solid or liquid phase, depending on the environmental temperature, without simulating the cloud formation process itself. Condensed methane is brought at the same timestep to lower levels as rainfall. At the gridpoint of condensation the methane mole fraction is lowered appropriately and the corresponding latent heat is released. Falling rain begins to evaporate as soon as it enters unsaturated levels. The amount of evaporation is such as to fill the saturation deficit. In case of evaporation latent heat is removed from the atmosphere. The remaining part of rain arrives at the surface and is removed from the atmosphere. We tacitly assume that sufficient condensation nuclei are present in the troposphere.

This case represents one of the usual approaches in terrestrial GCMs concerning the condensation in a supersaturated but statically stable region, and is known as "large-scale condensation," "supersaturation rain," or "stable condensation" in the climate modeling community in contrast to the cumulus convection. This condensation is usually correlated with stratiform clouds.

The model also contains a methane source at the surface in the form of surface evaporation. The surface evaporation (methane flux) is calculated by a bulk formula, which is used in some

terrestrial GCMs, anaglogously to the evaporation of water from Earth's surface. The flux depends on fundamental meteorological/hydrological parameters near the surface such as methane saturation deficit and wind speed in the surface layer (ventilation effect) as well as the moisture availability parameter, which varies from 1 (for ocean) to 0 (for desert).

In ignorance of the surface state and type of methane source on Titan we do not apply a more sophisticated scheme. For simplicity we arbitrarily assume a uniform moisture availability parameter of 0.5 without further specifying the type of methane source. This value should be justified since, to our current knowledge, neither a global methane ocean (parameter of 1) nor a total lack of methane sources (parameter of 0) is likely on Titan.

The mathematical formulation of condensation and evaporation is described in the Appendix.

Case 2: Condensation at saturation ratios exceeding 150%. This case differs from Case 1 in that condensation is allowed only when the saturation ratio at any gridpoint exceeds the critical value of 150%. Therefore, both supersaturation and condensation may exist to some extent. This concept is based on the aforementioned (Section 2) idea of the critical saturation ratio for hydrocarbons by Moses *et al*. (1992). This critical saturation ratio has been chosen arbitrarily, but in rough agreement with the maximum supersaturation inferred by Samuelson *et al*. (1997).

In case of condensation all excess portions of methane are immediately condensed out, so the saturation ratio at this particular gridpoint drops immediately to unity at this timestep. This may occur when aerosols with low surface energy acting as condensation nuclei receive a layer of condensed material with higher surface energy, leading to the avalanche condensation of all supersaturated species (Guez *et al*. 1997). As long as the falling rain passes levels with saturation ratios between 100 and 150% neither further condensation nor evaporation occurs, but it evaporates at unsaturated levels analogously to Case 1. This assumption is perhaps an unrealistic oversimplification. In reality falling raindrops and hailstones themselves act as condensation nuclei, so some supersaturated methane vapor would have to be removed below the initial condensation level as well. Possible deficiencies of our model are discussed in Section 5.

In contrast to Case 1 surface evaporation of methane is omitted because there is no surface precipitation as shown in Section 4.4.

4. RESULTS

Each scenario is simulated for two Titan years, starting from a resting atmosphere and the vertical temperature and methane profile after Lellouch *et al*. (1989). We adopt Lellouch *et al*. (1989) instead of Yelle *et al*. (1997) because the radiation model of McKay *et al*. (1989) used in our GCM is tuned to reproduce atmospheric parameters of Lellouch *et al*. (1989). The initial column methane abundance turns out to be 2661 kg m^{-2} and the global total mass of gaseous methane 2.22×10^{17} kg. The stratospheric circulation is also included in this GCM but not systematically analyzed since it is out of the scope of this paper and several stratospheric processes such as haze microphysics and photochemistry are not taken into account in this study.

4.1. General Circulation

The thermally direct meridional circulation (Hadley circulation) is a consequence of the global imbalance of the diabatic heating rate resulting from the differential insolation and inhomogeneous distribution of atmospheric opacity and temperature. The pattern of the meridional circulation is largely determined by the spatial distribution of the net diabatic heating rate unless dynamic instabilities distort the mean circulation. Net heating causes upwelling, while net cooling causes downwelling.

On slowly rotating planets on which no baroclinic instability arises the meridional circulation is thought to resemble the classical Hadley circulation proposed by George Hadley in the 18th century, i.e., rising motion at low latitudes, sinking motion at high latitudes, and compensating meridional flows in between. Venus indeed seems to possess such a circulation pattern (Schubert 1983). However, in contrast to Venus, Titan exhibits a marked seasonality due to the obliquity of Saturn (26.7°), so the subsolar latitude periodically oscillates between the northern and southern hemisphere. Therefore, Venus-like equator-to-pole cells are found in Titan's troposphere only around the equinoxes (Fig. 1). In most of remaining seasons one finds a global pole-to-pole cell with upwelling on the summer hemisphere. The only exception is the small equator-to-pole cell on the summer hemisphere in the lowest 5–15 km, where the net diabatic heating rate barely varies with season. The mass flux (so-called mass stream function) depicted in Fig. 1 is calculated from the mean meridional and vertical winds using the continuity equation. The mass flux indicates the mean overturnings of the mass in a meridional–vertical plane in which the air moves along the isolines. If, in contrast to our assumption, the ground temperature varied with season, we would expect a more asymmetric meridional circulation down to the surface as shown in Fig. 6 of Hourdin *et al.* (1995). In that case the zonal circulation may also be different because of the different transport pattern of angular momentum by the Hadley circulation.

Flasar *et al.* (1981) supposed that the seasonally independent part of the Hadley circulation would extend up to the tropopause. The discrepancy between our result and that of Flasar *et al.* (1981) may be explained by the difference in the radiative time constant. It is possible that the radiative time constant of Flasar *et al.* (1981) is larger than that resulting from the radiation model of McKay *et al*. (1989) used in our GCM. We also note that the sensible heat flux from the surface, which is subject to considerable uncertainty, does affect the diabatic heating rate.

Figure 2 shows that the net radiative heating rate in Case 1 has two maxima and a pronounced minimum at 12 km altitude, while this is not the case in Case 2. In Case 1 more sunlight penetrates the lower troposphere due to the low methane opacity in the mid-troposphere. Therefore, the solar heating rate has a distinct

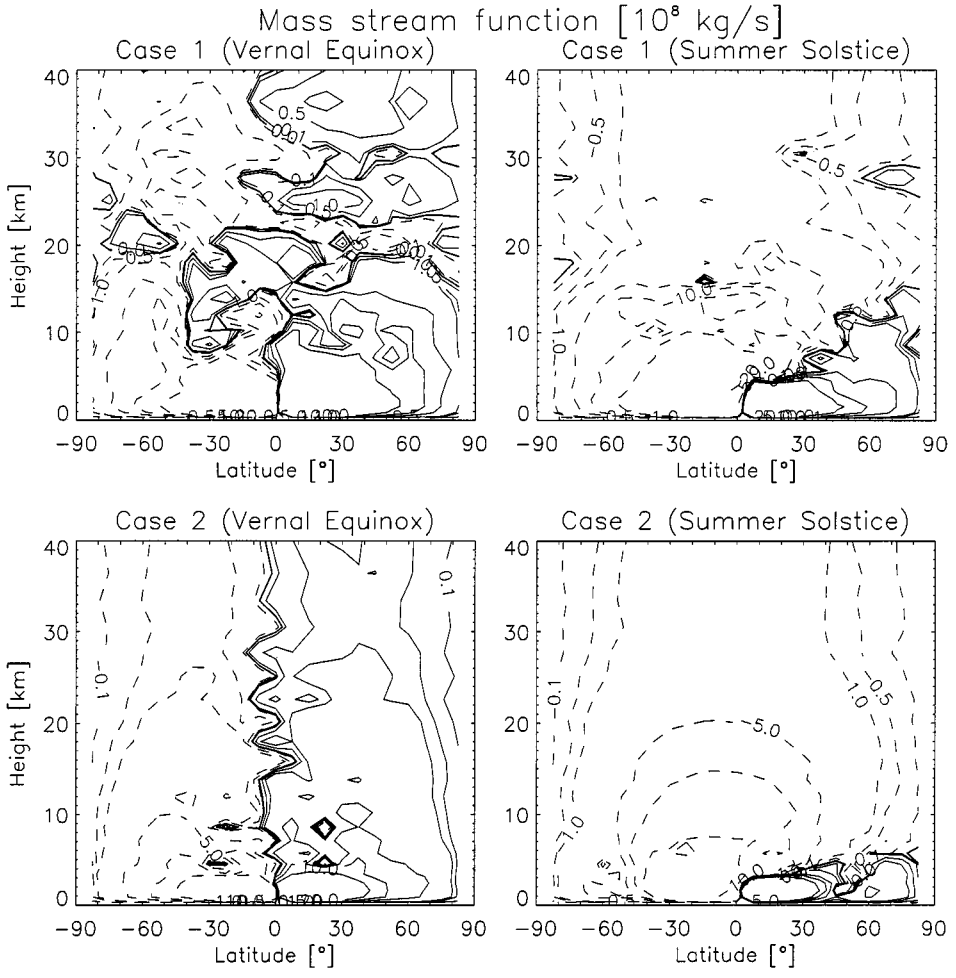

FIG. 1. Meridional circulation (Hadley circulation) respresented by the mass flux (mass stream function) (10^8 kg s^{-1}) at two seasons. The air flows along the streamlines, where solid and dashed curves indicate clockwise and anticlockwise circulation, respectively.

maximum at 8 km, while it is smaller by 50% at 20 km. At the same time the net thermal cooling rate is also weaker in the mid-troposphere due to the low temperature and low methane abundance. The superposition of this heating and cooling results in the net heating rate distribution of Fig. 2. Due to this split heating rate pattern the meridional circulation looks distorted. One can find several smaller cells inbedded in the equator-to-pole cells or the global cell.

In contrast to this the net radiative heating rate in Case 2 has only one distinct peak (0.008 K per Titan day) at 8 km because the methane abundance and hence the greenhouse effect are larger. One can clearly recognize equator-to-pole cells at the equinox and a pole-to-pole cell in the remaining seasons.

Since the diabatic heating is weak in Titan's troposphere ($<10^{-7}$ K s^{-1}) compared to the Earth, the strength of the circulation (at most 2×10^9 kg s^{-1}) is weaker than on Earth (at most 2×10^{11} kg s^{-1}, Peixoto and Oort (1992)) despite the larger atmospheric mass. The meridional and vertical wind speeds in the troposphere are on the order of 1 and 0.01 mm s^{-1}, but are one or two orders of magnitude larger in the vicinity of the intertropical convergence zone (ITCZ) near the equatorial surface.

One interesting finding is that also the development of the zonal circulation is sensitive to the methane distribution. This is because the Hadley circulation is greatly responsible for the formation, maintenance, redistribution, or decay of the zonal jets by the transport of angular momentum. Figure 3 depicts the latitudinal–vertical distribution of the zonal wind at the northern vernal equinox two Titan years after the start. In Case 1 the zonal wind is everywhere prograde (eastward) except near the equatorial surface. Initially a pair of distinct jets develops at about 50° latitude, 8 km altitude of both hemispheres, but after one Titan year the mid-latitude jets begin to decay, while the equatorial circulation slightly grows. The development ultimately stops after 1.5 Titan years and the result shown in Fig. 3 is also the final state. The maximum zonal wind speed in the troposphere is 3 m s^{-1}, and is found in a broad region at 10 km between 60°S and 60°N. No seasonal variation can be recognized.

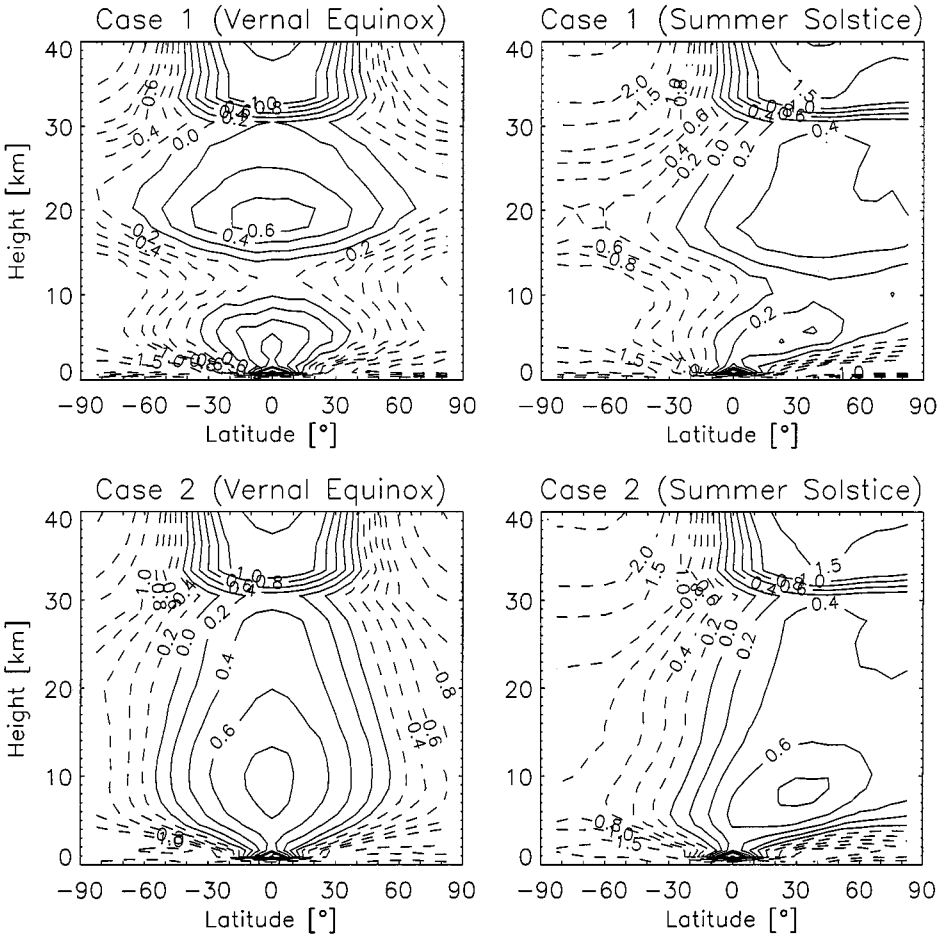

FIG. 2. Net radiative heating rate (0.01 K per Titan day) at the vernal equinox. Solid and dashed curves indicate net heating and net cooling, respectively.

In Case 2 the zonal circulation exhibits a pair of tropospheric jets at about 60° latitude, 10 km altitude, that periodically increases in local winter due to the poleward angular momentum transport by the small equator-to-pole cell in the summer hemisphere. Unlike Case 1 the zonal circulation continues to increase after two Titan years. This difference is likely to be found in the structure of the Hadley circulation, which consists of larger cells with a more efficient angular momentum transport.

4.2. Temperature

The temperature distribution in Titan's troposphere is quite uniform in the horizontal (Fig. 3). The equator-to-pole contrast is always less than 1 K except near the surface where the latitudinal variation is larger (up to 2 K close to the surface) due to the sensible heat flux from the surface. The reason for this latitudinally uniform temperature distribution is the tiny radiative heating rate in the troposphere compared to the heat transport process. However, the simulated equator-to-pole contrast near the surface is somewhat smaller than the contrast of about 4 K obtained from the *Voyager* data by Samuelson *et al.* (1997) and predicted by an application of the maximum entropy production principle to Titan (Lorenz *et al.* 2001), so this discrepancy might indicate a surface–atmosphere coupling on Titan stronger than that simulated in the GCM.

The longitudinal temperature distribution is almost uniform but with small variations (less than 1 K) associated with the latent heat release at some gridpoints due to condensation. Diurnal variation cannot be recognized. The only noteable seasonal variation is that caused by the orbital eccentricity of Saturn. Due to the slow radiative response of the troposphere the maximum temperature in the main part of the troposphere is observed about one season after the perihelion, i.e., close to the northern vernal equinox. In the mid-troposphere the difference between these two seasons is typically 0.5 K.

However there is also another temperature change associated with the methane depletion. The loss of methane has a serious consequence for the temperature since the greenhouse effect will be reduced. For instance at a thermal wavelength of 66.7 μm,

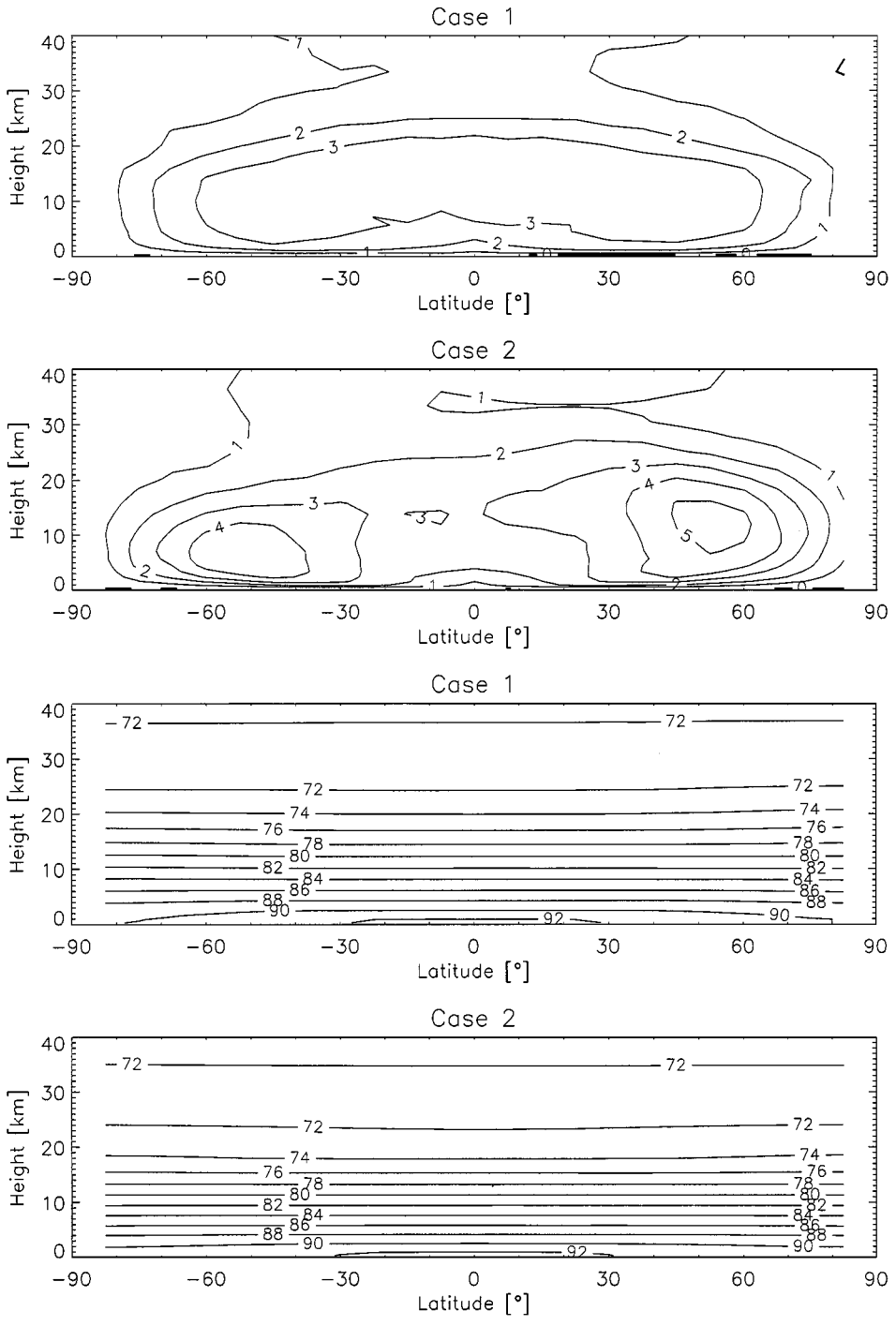

FIG. 3. Zonal wind u (m s^{-1}) (upper panels) and temperature T (K) (lower panels) in the troposphere at the vernal equinox two Titan years after the start. Solid and dashed curves of u indicate westerlies and easterlies, respectively.

at which the collision-induced absorption by the molecule pairs CH_4–CH_4 is strongest, the column optical depth declines from 25 at the beginning to less than 20. Since the radiative time constant in the mid-troposphere is more than one Titan year (Flasar *et al.* 1981, Tokano *et al.* 1999), the temperature decrease is not sudden, but a noteable drop can be observed from the second Titan year on. After two Titan years the temperature at 15 km is 2 K lower than at the beginning (Fig. 4). Nevertheless, the horizontal temperature variation remains small regardless of the methane abundance.

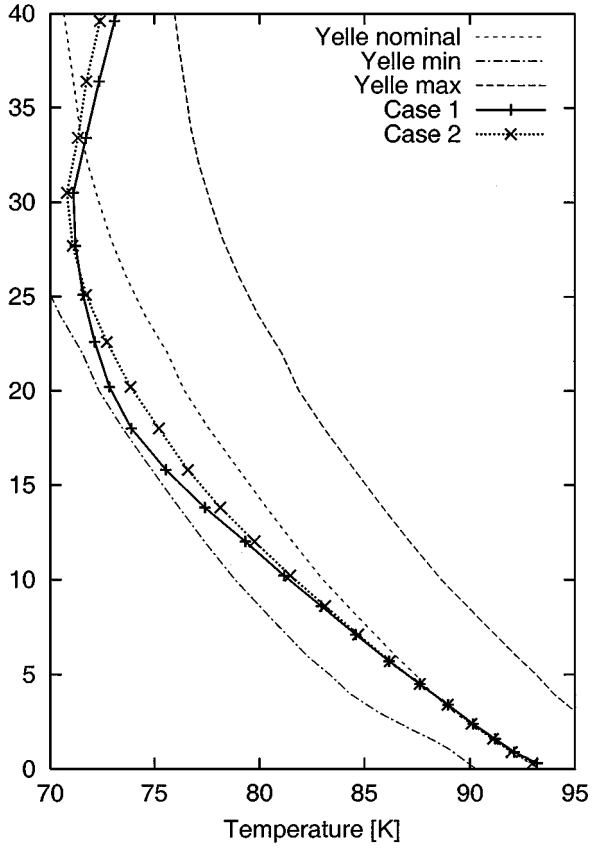

FIG. 4. Vertical temperature profile at the equator at the vernal equinox.

This kind of temperature drop is negligible in Case 2 since the methane abundance in the mid-troposphere does not decrease.

4.3. Methane distribution

The transport of methane in Titan's troposphere may be regarded as a combination of upward diffusion, downward precipitation, and three-dimensional advective transport. In contrast to diffusion and precipitation the direction of the advection depends on location and season.

Case 1. In the entire troposphere methane is subject to zonal, mostly eastward transport. The meridional–vertical transport is much slower than the zonal transport. Methane mostly circulates in the lower troposphere where the Hadley circulation is strong and the methane mole fraction is high. Below an altitude of 2 km methane is advected equatorward on both hemispheres and then upward near the equator. This feature is analogous to the terrestrial trade winds at low latitudes, which advect water vapour equatorward. The upward transport is effectively limited by condensation, which will be discussed in the next subsection.

The most obvious feature concerning the total methane inventory in Case 1 is its permanent loss (about 15% during the fist Titan year) caused by surface precipitation. The surface evaporation of methane is not sufficient to replenish the loss of atmospheric methane by precipitation during the first Titan year. Such a result is obviously not consistent with the present rich abundance of methane in Titan's troposphere (see also the discussion in Section 5).

Figure 5 shows the vertical profile of methane mole fraction and saturation ratio (relative humidity) at the equator. It is clear that the saturation ratio is limited to 100% and this limit controls the vertical methane distribution. Since the meridional distribution of temperature and the air pressure are quite uniform in the troposphere, the saturation vapor pressure barely varies with latitude and hence the methane mole fraction shown is found also at other latitudes. The methane mole fraction continuously decreases with altitude, but a minimum at 20 km is found after two Titan years. This minimum is not a direct result of condensation, which does not occur at this level, but is caused by advection. The stratospheric methane mole fraction of 1.5% does not change during the simulation since there are neither sources nor sinks in the model. The Hadley circulation does not cause any intrusion of methane into the stratosphere. Initially the saturation ratio is close to unity in a large part of the troposphere, but in the course of simulation, as the total methane inventory shrinks, saturated regions disappear in the mid-troposphere.

As a whole the global methane distribution in Case 1 does not undergo a systematic seasonal variation but a permanent loss due to the precipitation until the entire troposphere becomes so dry that no further surface precipitation falls. The simulation shows that it is not possible to maintain the initial methane profile of Lellouch *et al.* (1989) by a cycle of condensation and evaporation in the presence of atmospheric circulation.

Case 2. However, the situation changes in Case 2. One important difference to Case 1 is the fact that the upward methane transport is not limited by saturation (saturation ratio of 100%), but by a higher threshold (saturation ratio of 150%). This relaxed condition enables more methane to be carried into the mid-troposphere by both eddy diffusion and Hadley circulation. Since in Case 2 (Section 4.4) the atmospheric precipitation does not reach the surface, no loss of atmospheric methane takes place. A balance between upward transport by diffusion and advection and downward transport by precipitation is found, so a smooth vertical methane profile is established. The methane mole fraction continuously decreases with altitude, but the vertical gradient is smaller than in Case 1 (Fig. 5). This is because the condensation and rainfall, which would otherwise redistribute methane downward, are much less than in Case 1. The transport processes tend to establish a vertically uniform methane distribution, with a small limitation in the mid-troposphere by condensation.

However, substantial seasonal latitudinal transport is superposed on this vertical methane cycle. In the mid-troposphere, where the meridional circulation is mostly interhemispheric except at the equinoxes (Fig. 1), methane is subject to transport from the winter to summer hemisphere because more methane is available in the lower troposphere, i.e., in the lower branch of the interhemispheric Hadley cell. Associated with this transport is a periodical oscillation of the methane mole fraction

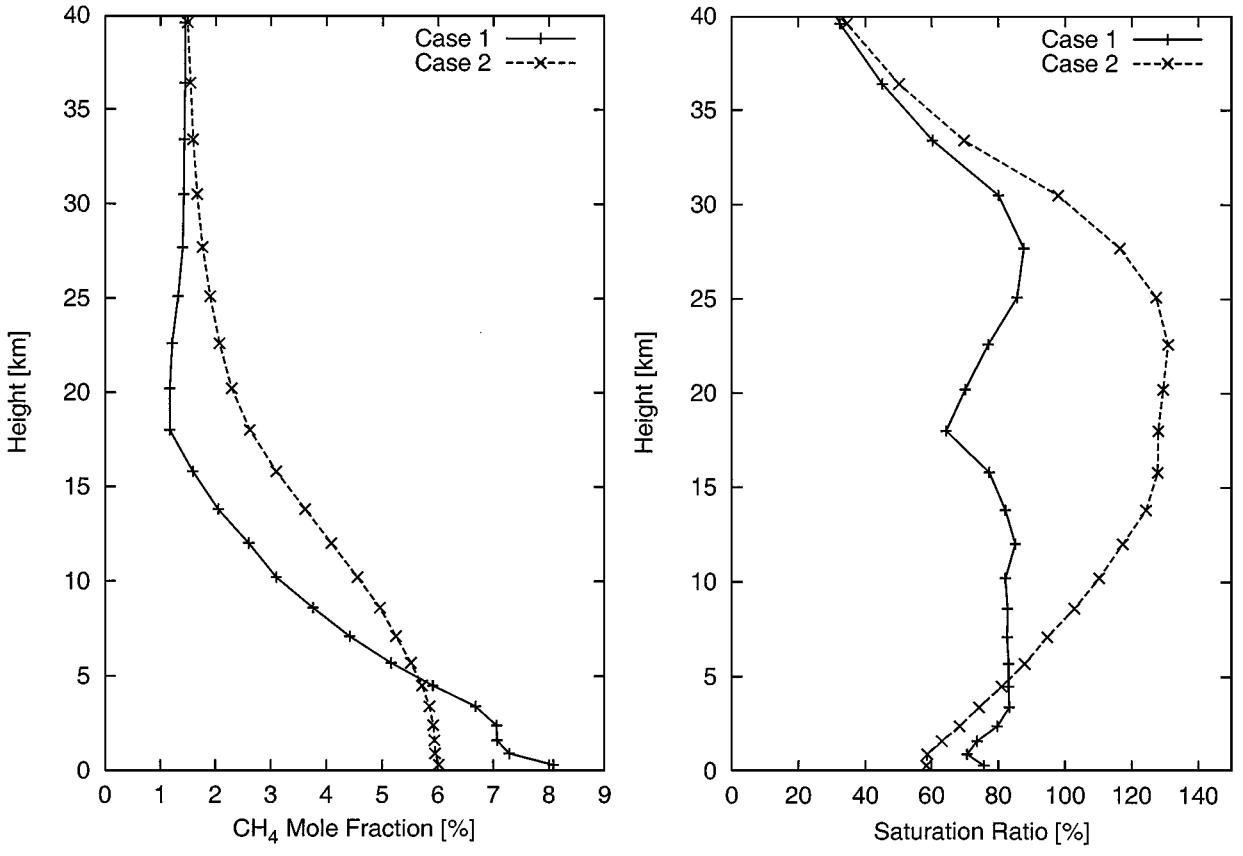

FIG. 5. Equatorial profile of the methane mole fraction and saturation ratio in Cases 1 and 2 at the vernal equinox two Titan years after the start.

and saturation ratio in the mid-troposphere with season (Figs. 6 and 7). In the mid-troposphere at mid-latitudes the methane mole fraction varies by 10 to 20% and the maximum is found in mid-summer. Figure 7 better illustrates how the column abundance of methane latitudinally and seasonally varies. At the equinox the maximum column abundance is found between the equator and 30° of the autumn hemisphere. The latitudinal decrease is larger on the spring hemisphere. At the solstice the column abundance continuously increases from the winter pole to the summer pole.

The seasonal variation of the saturation ratio, on the other hand, is not exactly correlated with that of the methane mole fraction since the temperature variation caused by the orbital eccentricity of Saturn also affects the saturation ratio. The tropospheric temperature becomes lowest near the northern autumnal equinox ($L_S = 180°$) and hence the highest supersaturation ratio is found near the autumnal equinox, i.e., half a season later than the maximum of the methane mole fraction. The maximum supersaturation on the southern hemisphere at the northern vernal equinox ($L_S = 0°$) is less pronounced, but still higher than on the opposite hemisphere.

Figure 8 shows that the troposphere between about 10 and 30 km is always supersaturated. The maximum supersaturation is about 135%, and is located at 22 km altitude, but its latitudinal location moves with the seasons. The supersaturation is systematically higher on the summer and autumn hemispheres. At all seasons the saturation ratio decreases at high latitudes, which is not owing to the methane loss by precipitation, but to the downward transport of methane-poor air near the poles by the Hadley circulation.

One might wonder why the maximum supersaturation is only 130% but not 150% (the upper limit), although this threshold will obviously be reached. The displayed values are zonal and temporal (10 Titan days) averages. The saturation ratio does occasionally exceed the threshold value of 150% at specific locations, but subsequent condensation immediately reduces the saturation ratio to unity, so the average values are always below the threshold.

The simulated variation of the methane abundance also causes a variation of the atmospheric opacity relevant for radiative heating and cooling. In the visible spectrum represented by the column optical depth at 0.64 μm the opacity is dominated by the stratospheric haze. Therefore, the opacity variation due to the inhomogeneous methane distribution is much smaller than that caused by haze transport (see also Tokano *et al.* (1999)). Note that in this GCM simulation the haze opacity is held constant. The opacity in the thermal infrared, on the other hand, is a superposition of several collision-induced absorptions (greenhouse effect) mainly in the lower troposphere. At 13.5 μm

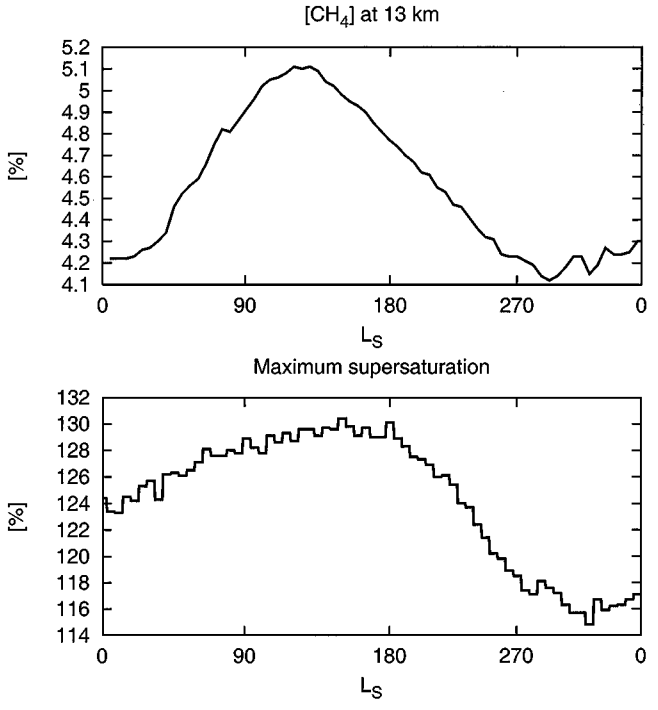

FIG. 6. Seasonal variation of the methane mole fraction at 13 km altitude at 45°N and the maximum supersaturation at the same latitude in Case 2. The steps in the bottom panel are caused by the averaging over 10 Titan days. L_S denotes the Kronocentric longitude of the Sun, with $L_S = 0^\circ$ at the northern vernal equinox, $L_S = 90^\circ$ at the summer solstice, etc.

(739 cm^{-1}), where absorption by H_2–N_2 dominates, the column optical depth increases with latitude by about 15% because the methane abundance decreases with latitude and nitrogen abundance increases proportionally. At 66.7 μm (200 cm^{-1}), where absorption by CH_4–CH_4 and CH_4–N_2 is strong, the column optical depth exhibits a large decrease with latitude with an equator-to-pole contrast of roughly 50%. This directly reflects the global methane distribution and the vast importance of methane to the greenhouse effect in this spectral region. At 200 μm (50 cm^{-1}), where N_2–N_2 absorption constitutes about 80% of the opacity and CH_4–N_2 about 20%, the latitudinal variation of the column optical depth is at most 2%.

4.4. Condensation and Precipitation

Case 1. The upper panel of Fig. 9 depicts the global distribution of the total condensation amount in Case 1 in the first Titan year. Condensation takes place wherever the air becomes supersaturated. The maximum condensation amount is found in the lower troposphere near 3 km altitude near the equator because this region most frequently becomes saturated by the strong methane supply from below correlated with intertropical convergence. Supersaturation is being always removed instantaneously by condensation, but is soon established by zonal methane transport from the neighbor region. The amount of condensation at each timestep is small, corresponding to a saturation excess of typically less than 1%. Therefore, the latent heat released during the condensation is not significant, and will soon be smoothed out by zonal advection. The latent heat is by far not capable of preventing a temperature drop caused by the reduced greenhouse effect.

At all altitudes the annual condensation decreases with latitude because the upward methane transport, which represents an important process for the maintainance of condensation in the mid-troposphere, is strong at low latitudes but less so at high latitudes. This is closely correlated with the meridional structure of the Hadley circulation. Since the simulated ITCZ does not shift seasonally, the condensation takes place throughout the year with a weak seasonality. The condensation at high latitudes is confined to the lowest few kilometers while at low latitudes it occurs up to an altitude of 25 km, but the contribution of the high-altitude condensation to the total precipitation amount is small. In this region the temperature is lower and condensation sets in at lower methane mole fractions, but the condensation amount is much smaller than at low altitudes. On the other hand, condensation does not occur below 2 km in the equatorial region because this area remains dry.

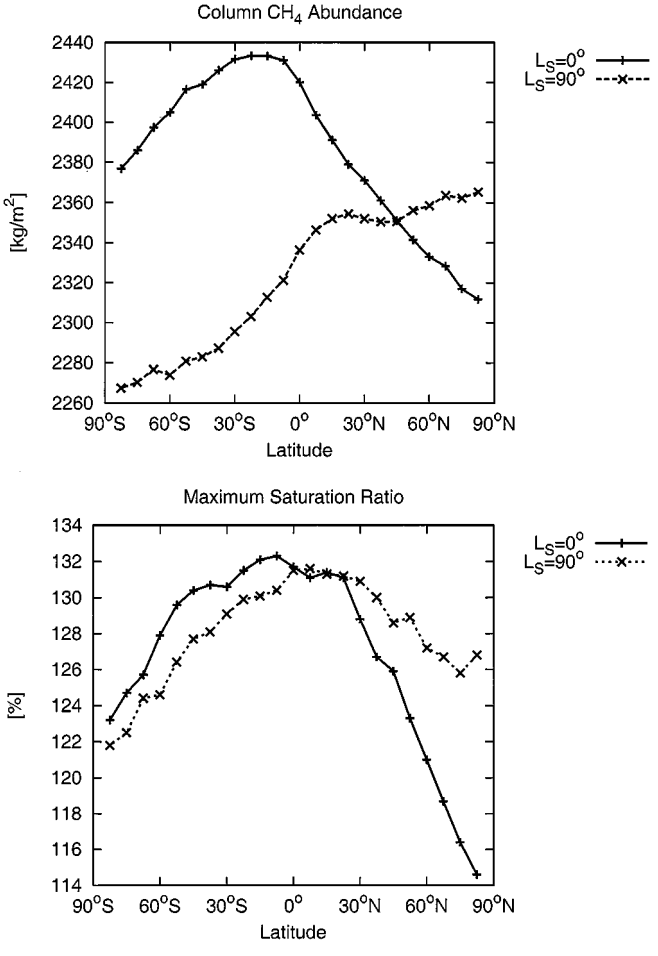

FIG. 7. Latitudinal distribution of column (vertically integrated) methane abundance (kg m^{-2}) at two seasons in Case 2.

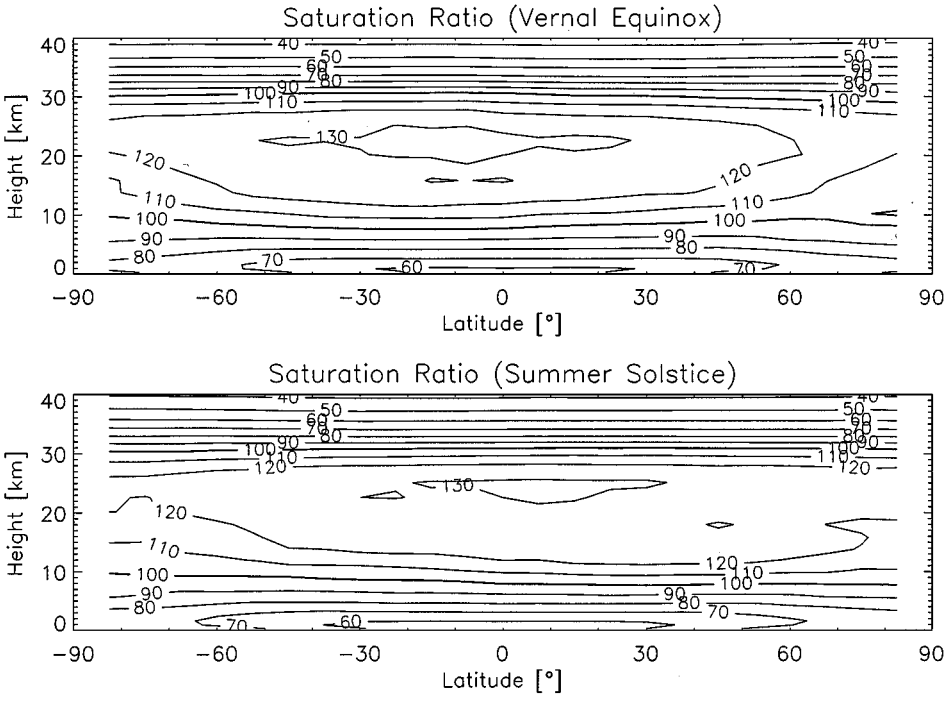

FIG. 8. Global distribution of saturation ratio (%) at two seasons in Case 2.

The surface precipitation rate is not controlled by the season, but is basically dependent on the latitude, and is rather symmetric about the equator (Fig. 10). The annual surface precipitation peaks at the equator (9500 kg m^{-2} per Titan year or 10^{-5} kg m^{-2} s^{-1} or about 640 mm per Earth year) as a result of strong convergence typical for the ITCZ. The surface precipitation rapidly decreases with latitude, and at the remaining low latitudes between 10° and 30° of both hemispheres only 10% of

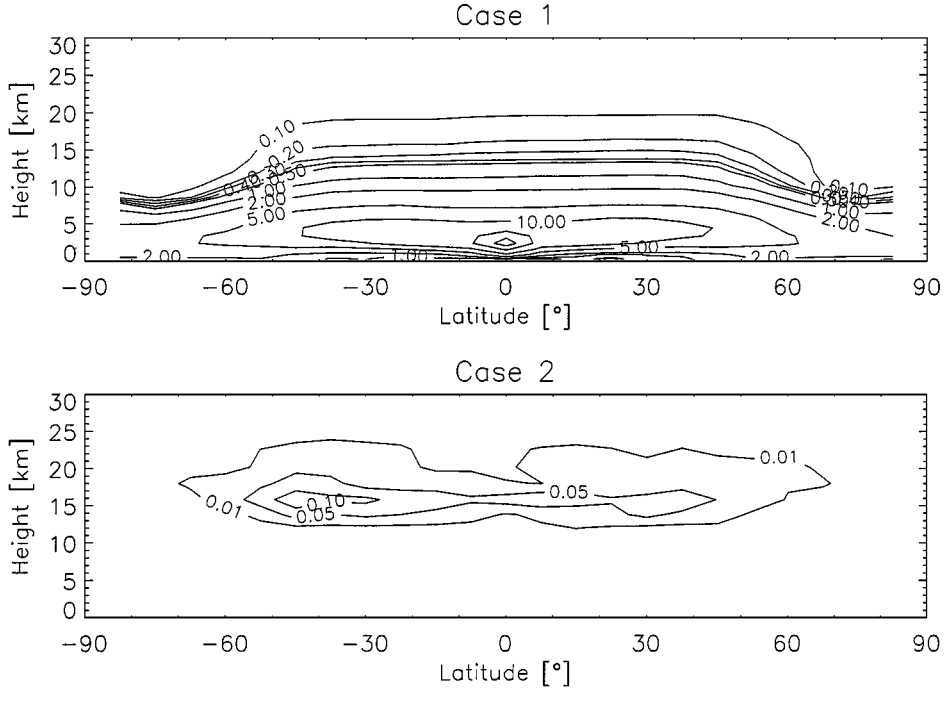

FIG. 9. Total condensation amount (kg m^{-3}) per Titan year for Cases 1 and 2.

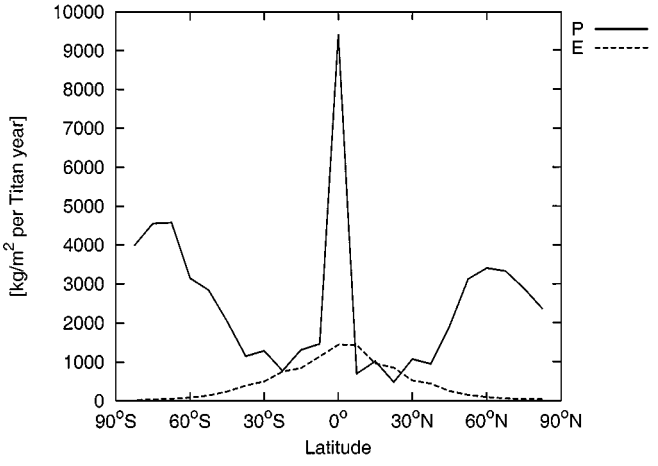

FIG. 10. Total surface precipitation P and evaporation E (kg m^{-2}) per Titan year for Case 1. If one multiplies the values by 4, one gets approximately the precipitation rate in millimeters per Earth year. No surface precipitation is observed in Case 2.

the equatorial surface rain is measured. The surface precipitation increases at mid-latitudes and peaks again between 60° and 70°. The global-mean surface precipitation rate is 1483 kg m^{-2} s^{-1} per Titan year (1.6×10^{-6} kg m^{-2} s^{-1}, 100 mm per Earth year), and is about 10 times smaller than that on Earth.

It is quite interesting that the annual surface precipitation increases with latitude, although the total condensation decreases with latitude, with the small exception at the equator. At low latitudes the condensation level is higher and hence falling rain has more chance to evaporate, while at high latitudes rain produced near the surface cannot substantially evaporate. Since the temperature of the condensation levels is mostly above 80.6 K, the freezing point of a binary mixture of methane and nitrogen, condensed methane with a small amount of dissolved nitrogen, should be liquid.

The rainfall at the surface is quite continuous, but the annual rainfall is somewhat higher on the southern hemisphere. We ascribe this feature to the small temperature seasonal variation caused by Saturn's eccentricity, but do not scrutinize it since the (arbitrary) initial methane distribution does also affect the result. We remark that in general the precipitation (at the surface) is one of the most uncertain variables in GCMs because it depends on many factors such as temperature, mole fraction, efficiency of evaporation, and model schemes. In the case of Titan the difficult efficiency of nucleation and the steep temperature dependence of the saturation vapor pressure of methane compared to that of H_2O in the terrestrial troposphere further enhance the uncertainty.

The surface evaporation of methane, on the other hand, is also permanent and is also primarily a function of latitude. It decreases from 1400 kg m^{-2} per Titan year (1.5×10^{-6} kg m^{-2} s^{-1}) at the equator monotonically to zero at the poles. We assumed evaporation to be proportional to the saturation deficit (Eq. (12)); i.e., there is more evaporation in a dry atmosphere (equator). The global-mean evaporation rate at the surface is 409 kg m^{-2} per Titan year (4.4×10^{-7} kg m^{-2} s^{-1}, 28 mm per Earth year). Hence, the sink (rain) is 3.6 times larger than the source (evaporation) in the first Titan year. In the second Titan year condensation declines because almost nowhere the atmosphere is saturated after the heavy rainout. The surface evaporation, on the other hand, continues.

As already mentioned in Section 2 we are not aware of the type and strength of methane source or methane evaporation on Titan. The bulk formula used in the GCM for the calculation of surface evaporation can be applied to different source types (ocean, lakes, solid surface) if an appropriate moisture availability parameter M is defined (see the Appendix). Since M on Titan is unknown, we arbitrarily assumed $M = 0.5$, which rules out a global ocean or "desert." In the case of a global ocean ($M = 1$) Eq. (12) indicates a double (and maximum) evaporation rate, but an evaporation rate of 800 kg m^{-2} per Titan year could still not replenish the precipitation rate. We note that several parameters in Eq. (12) are unconstrained, so the calculated evaporation rate is uncertain.

From a climatological point of view the latitudinal distribution of precipitation needs not to coincide with the distribution of evaporation, but the annual global precipitation should be balanced by the annual global evaporation in order to maintain the hydrological cycle. The result of Case 1 seems to indicate that a stable hydrological cycle of methane is difficult to maintain on Titan regardless of the surface type if a critical saturation ratio of 100% for the onset of condensation is assumed.

Case 2. The results of Case 2, on the other hand, show many differences to Case 1. In keeping with the high critical saturation ratio of 150%, the amount of condensation in this case is greatly reduced compared to Case 1. The accumulated condensation amount per unit volume of air (Fig. 9) is at most $\approx$0.1 kg m^{-3} per Titan year, roughly two orders of magnitude less than in Case 1. A higher critical saturation ratio has thus the effect to reduce the total condensation amount, although the amount of condesation per event, corresponding to a saturation excess of 50%, is much larger. The typical temperature increase due to the latent heat release is 3 K. This temperature anomaly will soon be smoothed by zonal heat transport, so no systematic longitudinal variation is present.

Most condensation occurs at low and mid-latitudes at 15 km altitude, i.e., 10 km higher than in Case 1. This is the location where the saturation ratio most frequently exceeds the threshold value of 150%. Condensation in other regions of the troposphere is almost negligible. Condensation occurs preferentially in late summer and early autumn when the supersaturation becomes highest due to the enhancement of methane by seasonal transport from the opposite hemisphere. Since after the condensation the saturation ratio at this specific location immediately drops to unity, it takes several Titan days until at this gridpoint the supersaturation is established again by advection of humid air. Hence, the condensation is always discontinuous. A further important difference to Case 1 is that the entire precipitation evaporates in

the lower troposphere, so not a single raindrop arrives at the surface, provided the surface has no topography. As already mentioned in Section 4.3 this has an important consequence that the total atmospheric methane inventory is conserved (except for the photochemical destruction not considered in this study), and the simulated methane hydrological cycle occurs *within* the atmosphere rather than in the atmosphere–surface–subsurface system.

5. DISCUSSION

5.1. Methane Distribution and Condensation

In the previous subsections the results of both cases have been presented and compared with each other. Here, we attempt to verify these results, so far it is possible, by comparisons with observational data in order to interpret them. As already mentioned in Section 2, data about methane on Titan are scarce and uncertain, but there are some indications that can be utilized. The latitudinal distribution of some methane-related quantities at the time of *Voyager 1* flyby was inferred from the IRIS spectra by Samuelson *et al.* (1997) by computing synthetic spectra for various combinations of parameters to fit the observed IRIS spectra. They were able to derive the most likely maximum saturation ratio within each vertical column of air at nine latitudes sampled by IRIS. They introduced a parameter ΔT (constant temperature difference that is added to the temperature profile to create another profile in the radiation code) as a device for introducing supersaturation in their model. The data were calculated under the assumption that the tropopause temperature and stratospheric haze opacity at wavenumber 530 cm^{-1} were latitudinally uniform. They calculated the vapor pressure with respect to pure methane, which typically deviates by 20% from that with respect to the binary mixture of methane and nitrogen. The altitude of the maximum supersaturation was not determined, but these data provide the most powerful constraint on the methane condensation in Titan's atmosphere since they may give a hint on the possible critical saturation ratio. Although the data at high latitudes are uncertain, high supersaturation with saturation ratios between 140 and 165% was found at all nine latitudes between 60°S and 60°N. There was a slight tendency to higher supersaturation in the southern (autumn) hemisphere and to a decrease toward both poles (upper panel of Fig. 11).

The result of Case 1 is incompatible since no supersaturation is allowed at all.

The curve of Case 2 shows a relatively high saturation ratio of 132% in a wide region around the equator. Despite a quantitative discrepancy to Samuelson *et al.* (1997) the latitudinal shape, i.e., higher supersaturation on the southern hemisphere and smooth latitudinal variation near the equator and a decrease at high latitudes, is roughly reproduced. It seems that a somewhat higher critical saturation ratio in the model could reproduce a better fit to the observation.

The obtained distribution should rule out a latitudinally uniform methane distribution in the highly supersaturated mid-

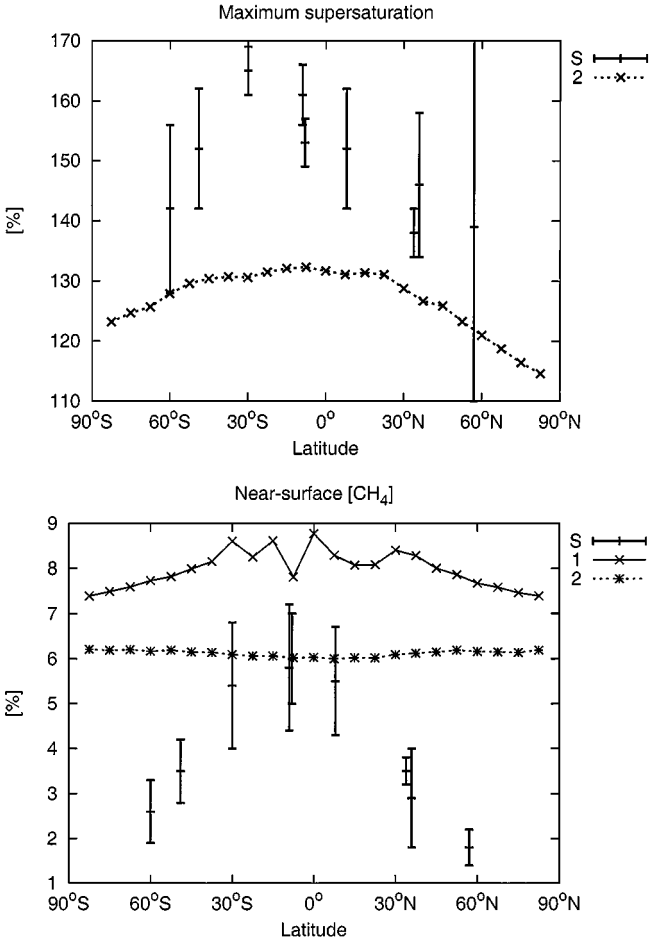

FIG. 11. Latitudinal methane distribution at the time of *Voyager 1* simulated by the GCM and retrieved by Samuelson *et al.* (1997). The upper panel shows the maximum supersaturation and the lower panel shows the near-surface methane mole fraction. "S" denotes the data after Samuelson *et al.* (1997); the numbers denote the simulated cases.

troposphere because otherwise the temperature at these levels would have to increase substantially with latitude, which is not the case. It is likely that not only the saturation ratio, but also the methane mole fraction decreases at high latitudes. This makes an important difference to the almost uniform methane distribution in the stratosphere simulated by Dire (2000).

An important result of this simulation is that the coexistence of condensation and substantial supersaturation appears necessary to explain the observed higher methane abundance in autumn. It is also remarkable that a latitudinally constant critical saturation ratio, whatever the exact value of this might be, causes a nonuniform latitudinal variation of supersaturation. This interesting feature is produced by an interplay of interhemispheric transport and condensation. Samuelson *et al.* (1997) and Samuelson and Mayo (1997) gave the following explanation for the general decrease of maximum supersaturation with latitude. They speculated that condensation and rainfall would occur preferentially at the spring pole where condensed ethane particles originating

from the cold spring stratosphere precipitate down into the supersaturated region and initiate efficient nucleation. They believed that the observed decrease of the maximum supersaturation toward the North Pole (spring pole) to be indicative of this effect.

Although we do not rule out the possiblity of condensation at the spring pole, our simulation shows that the observed latitudinal decrease and the hemispheric asymmetry can be produced naturally despite the occurrence of condensation at low latitudes. We emphasize that the Hadley circulation, both the symmetric one in the lower troposphere and the interhemispheric one at higher altitudes, significantly contributes to the observed methane distribution.

It is interesting that the presumable altitude of 15 km determined for the clouds found on 4 and 5 September 1995 (close to the northern autumnal equinox) at low latitudes (Griffith *et al.* 1998) coincides with the altitude, latitude, and season of maximum condensation in Case 2 of our simulation. This agreement would rather point to supersaturation rain for these clouds, while Griffith *et al.* (2000) themselves suggested a convective origin for the clouds found later in 1999. Since condensation occurs in a highly supersaturated region in the mid-troposphere, clouds cannot be maintained for a long time. Cloud particles would grow rapidly and immediately fall out as "rain without clouds" (Toon *et al.* 1988). This may explain the short life (less than 2 h) of clouds found by Griffith *et al.* (2000). However, the fact that Griffith *et al.* (2000) revised the original estimates of cloud altitude and global cloud coverage done by Griffith *et al.* (1998) shows that the cloud data are not very reliable at the moment, so we do not pursue the comparison with identified clouds.

Our present GCM can only account for large-scale supersaturation rain, which may well take place, but recent studies seem to indicate that different types of condensation occur on Titan. The first type may be the local, rapid cloud formation process responsible for clouds reported by Griffith *et al.* (1998, 2000). This is likely to occur at low latitudes and plenty of condensation nuclei would have to be present. These clouds may favor lightning generation (Tokano *et al.* 2001). The second type of condensation is that envisioned by Samuelson *et al.* (1997) and Samuelson and Mayo (1997), i.e., condensation relying on ethane particles that slowly precipitate down from the stratosphere. This condensation may preferentially take place near the spring pole. It is uncertain whether the results of our GCM represent either of these condensation types.

An appropriate treatment of different condensation processes in a GCM is a difficult task, even in terrestrial models. A reason for the difficulty is to handle different spatial and temporal scales of the processes in a GCM. Detailed one-dimensional models such as Guez *et al.* (1997) or Samuelson and Mayo (1997) may be better suited for studying the condensation processes themselves. Future condensation parameterizations in GCMs should take into account the information to be obtained from such models as well as further observational constraints.

The general message to be read from our study is therefore to recognize the importance of the relationship between the condensation, transport, and feedback to the general circulation rather than to predict the condensation on Titan.

Another key parameter derived by Samuelson *et al.* (1997) was the methane mole fraction just above the surface, also during the *Voyager 1* flyby (lower panel of Fig. 11). The values were remarkably symmetric about the equator, with about 6% near the equator and about 2% near 60° of both hemispheres.

The near-surface methane mole fraction predicted by the GCM in Cases 1 and 2 is also nearly symmetric about the equator, but the value does not agree with Samuelson *et al.* (1997). Case 1 shows a slight decrease from about 8.5% at the equator to about 7.4% at the poles. The value in Case 2 is about 6% everywhere without showing noteable latitudinal variation. The higher value in Case 1 is a result of surface evaporation and evaporation of falling rain near the surface. Since the predicted near-surface mole fraction in Case 1 is too high, we suggest that it is likely that the evaporation of falling rain should not occur near the surface but at much higher altitudes. The surface methane evaporation, which decreases with latitude, may in part explain the observed latitudinal decrease of the near-surface evaporation, but seems to be insufficient to cause a large decrease from 6 to less than 2%.

The equatorial value of Case 2 agrees quite well with Samuelson *et al.* (1997), so in combination with other constraints (supersaturation, cloud location) the modeled hydrological cycle at the equator may be realistic, i.e., condensation occurs in the mid troposphere, if any, and all rain evaporates in the mid troposphere, so the lower troposphere is not involved in the hydrological cycle. However, the near-surface methane mole fraction at other latitudes is too high, so some other mechanisms should be working since advection, condensation, evaporation, and combinations of them are not capable of producing the observed latitudinal decrease.

Samuelson *et al.* (1997) explained the remarkable latitudinal decrease of the near-surface methane mole fraction by a possible strong coupling of methane to the surface. If there are liquid hydrocarbon deposits on the surface, the methane mole fraction just above the liquid surface will be determined by the methane concentration in the liquid because of the thermodynamic equilibrium between the air and liquid. Since the polar hydrocarbon lakes may be enhanced in ethane (and thus diminished in methane) with respect to low-latitude lakes due to the ethane precipitation near the poles, the equilibrium methane near the surface will also decrease with latitude. The fixing of the polar temperature to the methane–nitrogen dew point as proposed by Stevenson and Potter (1986), on the other hand, requires a methane mole fraction of 7 to 8% at the polar surface, which is in sharp contrast to that of Samuelson *et al.* (1997). Although both groups assume some hydrocarbon ocean or lakes to support their own hypothesis, the assumed composition is different. Stevenson and Potter (1986) suggest a high methane concentration in polar lakes due to the large amount of condensed methane while Samuelson *et al.* (1997) suggest a higher ethane concentration there. In other words, it is not possible to fulfil both

hypotheses simultaneously with the observed latitudinal temperature and methane distribution.

5.2. Remarks

Our study is the first attempt to comprehensively model Titan's tropospheric methane cycle by a three-dimensional GCM. The processes and their parameterization in the model are quite simple, although we have tried to take into account all the major global effects (transport, condensation, source) we can imagine. There are several uncertainties and possible shortcomings of the model that could complicate the simple picture presented here.

The radiative effects of tropospheric clouds are not treated in the model. According to the radiation model of McKay *et al.* (1989) methane clouds introduce an additional opacity source in both the solar and thermal spectra, without windows and significant absorption bands. Due to the strong supersaturation in the mid-troposphere we do not support the presence of permanent methane cloud decks, and the condensation we have simulated may have no radiative effects considering the huge radiative time constant in Titan's troposphere.

We have not assumed any topography in our model since there is no certain observational evidence for mountains. If there are some mountains with heights of the order of kilometers, they may cause local or meso-scale features such as lifting of air with moist convection. Moreover, in contrast to the remaining parts of Titan, the precipitation may arrive at the surface of mountains. The critical saturation ratio for methane is sensitive to the physical properties of available condensation nuclei (Moses *et al.* 1992). At the spring pole solid ethane particles from the stratosphere may act as condensation nuclei (Samuelson *et al.* 1997), while the nuclei for the methane condensation at low latitudes are unknown. Since both types of particles may undergo seasonal variation, we cannot rule out that the critical saturation ratio depends on location and season.

6. CONCLUSIONS

The atmospheric methane cycle in Titan's atmosphere has been investigated by a three-dimensional atmospheric general circulation model. The model includes the advective and diffusive transport, condensation, precipitation, and evaporation of methane. Since the atmospheric conditions under which condensation occurs in Titan's troposphere is not well known, condensation is assumed to take place if the saturation ratio (relative humidity) exceeds either 100% (Case 1) or 150% (Case 2).

We have shown that the latter critical saturation ratio (150%) is more compatible with the *Voyager* data analyzed by Samuelson *et al.* (1997). The scenario enables high supersaturation in the mid-troposphere and allows only occasional condensation, so the loss of atmospheric methane by precipitation is negligible. The latitudinal shape of the maximum supersaturation resembles that retrieved from *Voyager* infrared spectral data except for a quantitative difference. It is suggested that the critical saturation ratio may be somewhat higher than 150%. The meridional circulation accounts for a seasonal transport of methane from the winter to summer hemisphere in the mid-troposphere, and causes a higher supersaturation in late summer and early autumn. Falling rain evaporates during the descent, so not a single raindrop arrives at the surface if there is no topography. Therefore, the hydrological cycle should take place mostly within the atmosphere. Nevertheless, some potential methane sources at the surface should be present since methane is subject to photochemical destruction in the upper atmosphere. We only suggest that methane sources are not necessary from a hydrological point of view.

The coincidence of location and season between the maximum condensation in the model and clouds spectroscopically identified by Griffith *et al.* (1998) is interesting, but further observation by different methods and theoretical research are necessary to investigate the nature of methane clouds on Titan.

On the other hand, Case 1 is less compatible with observation. It does not allow any supersaturation and does not cause a latitudinal methane distribution asymmetric about the equator, and the hydrological cycle is difficult to maintain on an annual basis. If immediate condensation were possible at saturation, the surface precipitation would be mainly dependent on latitude rather than on season.

In either Case 1 or Case 2 the latitudinal methane distribution near the surface cannot be reproduced by transport, evaporation, condensation, and combinations of them, so some additional undetermined surface processes should be operating.

The development and state of the zonal and meridional circulation are sensitive to the methane distribution due to a change in radiative heating rates. The Hadley circulation in the troposphere in Case 2 consists of large cells, while in Case 1 the circulation is split into many small cells because there are two maxima of the net radiative heating rate. The zonal circulation continuously increases in Case 2, but less so in Case 1 because the angular momentum transport by small cells is less efficient.

APPENDIX: CONDENSATION AND EVAPORATION

The changes in methane mole fraction C and temperature T due to condensation or evaporation are carried out at each timestep as adjustments prior to the calculation of other tendencies (advection, radiation, etc.).

The saturation ratio (relative humidity) of methane is defined as

$$\mathrm{RH} = 100\frac{p_{\mathrm{CH_4}}}{p^*_{\mathrm{CH_4}}}, \tag{2}$$

where $p_{\mathrm{CH_4}}$ is the vapor pressure of methane and $p^*_{\mathrm{CH_4}}$ the saturation vapor pressure.

The vapor pressure is the product of the total pressure p and the methane mole fraction C. $p^*_{\mathrm{CH_4}}$ is calculated by the formula of Thompson *et al.* (1992), considering the vapour–liquid equilibrium in a binary mixture of N_2 and CH_4.

The methane specific humidity is defined as the ratio of the mass of methane vapor to that of air

$$q = \frac{m_{\mathrm{CH_4}}}{m}\frac{p_{\mathrm{CH_4}}}{p} = 0.582C, \tag{3}$$

where $m = 27.5$ is the mean molecular weight of air and $m_{\mathrm{CH_4}} = 16$ is the molecular weight of methane.

The saturation specific humidity is then

$$q^* = 0.582\frac{p^*_{\mathrm{CH_4}}}{p}. \tag{4}$$

The excess specific humidity that condenses out at layer k is

$$\Delta q_k = q - q^*, \tag{5}$$

where q is always larger than q^* and therefore Δq is positive.

The amount of condensing and precipitating methane per unit area at a given layer k, P_k (kilogram per meter^2), is calculated as the mass of the excess fraction of methane

$$P_k = \frac{\pi}{g}\Delta q_k \Delta\sigma_k, \tag{6}$$

where π is the surface pressure, g is the gravitational acceleration, and $\Delta\sigma_k$ is the depth of the layer in the σ coordinate.

The amount of evaporation corresponds to the saturation deficit

$$E_k = \frac{\pi}{g}\Delta q_k \Delta\sigma_k. \tag{7}$$

If the passing rain is less than E_k, then all rain evaporates. The remaining portion of the rain is brought to the next lower layer. It is self-evident that condensation and evaporation do not occur simultaneously at a given gridpoint. The vertical sum of P_k before evaporation is P_0.

The surface rain P is P_0 minus the vertical sum of evaporated rain E_k

$$P = P_0 - \sum_{k'=1}^{KM} E_{k'}, \tag{8}$$

where KM = 60 is the total number of vertical layers.

The surface rain can also be expressed in precipitation height (meters), which is more common in the meteorology, by dividing P by the density of liquid methane under the conditions at Titan's surface, $\rho \approx 550$ kg m^{-3}.

The condensed portion of methane is removed from the atmosphere, i.e., the mole fraction C declines. This adjustment is done prior to the update of C by advection.

$$C_{\mathrm{after}} = C_{\mathrm{before}} - \frac{1}{0.582}\Delta q. \tag{9}$$

Analogously, the evaporated portion of rain is added to C.

At the same time the latent heat of condensation is added to or substracted from the air in case of condensation or evaporation, respectively. This adjustment is also done prior to the update of T by other effects

$$T_{\mathrm{after}} = T_{\mathrm{before}} + \frac{L}{c_p}\Delta q, \tag{10}$$

where L is the condensation enthalpy. L is positive for condensation and negative for evaporation. Due to the decrease of C and the increase of T, the air at this gridpoint is slightly subsaturated after this adjustment. The condensation enthalpy (latent heat) (joules per kilogram) is calculated as

$$\log_{10} L = (1.65214 + 2.0076 \times 10^{-4}(191.06 - T) + 0.22225\ \log_{10}(191.06 - T))4185, \tag{11}$$

which is approximately 5.6×10^5 J kg^{-1}.

The surface methane evaporation E_S (kilograms per meter^2 per second) is calculated by the bulk-aerodynamic formula of Deardorff (1972) analogously to the surface evaporation of water from the Earth's surface as

$$E_S = \rho_S C_U C_H (q^* - q) W_S M, \tag{12}$$

where ρ_S is the air density in the surface layer, $C_U = \sqrt{2 \times 10^{-3}}$ is the surface exchange coefficient for momentum, $C_H = 3 \times 10^{-3}$ is the surface heat exchange coefficient, both being typical terrestrial values for a smooth surface, W_S is the wind speed in the surface layer, and M is the moisture availability parameter, which is arbitrarily set to 0.5 in this study.

ACKNOWLEDGMENTS

This work is financially supported by the DLR (Deutsches Zentrum für Luft- und Raumfahrt). We thank Max J. Suarez (NASA/GSFC) for the source code of the GCM dynamical core. We appreciate useful suggestions by Robert E. Samuelson and another referee.

REFERENCES

Courtin, R., D. Gautier, and C. P. McKay 1995. Titan's thermal emission spectrum: Reanalysis of the Voyager infrared measurements. *Icarus* **114**, 144–162.

Coustenis, A., and B. Bézard 1995. Titan's atmosphere from Voyager infrared observations. IV. Latitudinal variations of temperature and composition. *Icarus* **115**, 126–140.

Deardorff, J. W. 1972. Parameterization of the planetary boundary layer for use in general circulation models. *Mon. Wea. Rev.* **100**, 93–106.

Dire, J. R. 2000. Seasonal photochemical and meridional transport model for the stratosphere of Titan. *Icarus* **145**, 428–444.

Flasar, F. M. 1983. Oceans on Titan? *Science* **221**, 55–57.

Flasar, F. M., and B. J. Conrath 1990. Titan's stratospheric temperatures: A case for dynamical inertia? *Icarus* **85**, 346–354.

Flasar, F. M., R. E. Samuelson, and B. J. Conrath 1981. Titan's atmosphere: Temperature and dynamics. *Nature* **292**, 693–698.

Fortes, A. D. 2000. Exobiological implications of a possible ammonia-water ocean inside Titan. *Icarus* **146**, 444–452.

Griffith, C. A., J. L. Hall, and T. R. Geballe 2000. Detection of daily clouds on Titan. *Science* **290**, 509–513.

Griffith, C. A., T. Owen, G. A. Miller, and T. Geballe 1998. Transient clouds in Titan's lower atmosphere. *Nature* **395**, 575–578.

Guez, L., P. Bruston, F. Raulin, and C. Régnaut 1997. Importance of phase changes in Titan's lower atmosphere. Tools for the study of nucleation. *Planet. Space Sci.* **45**, 611–625.

Hourdin, F., O. Talagrand, R. Sadourny, R. Courtin, D. Gautier, and C. P. McKay 1995. Numerical simulation of the general circulation of the atmosphere of Titan. *Icarus* **117**, 358–374.

Karkoschka, E. 1998. Methane, ammonia, and temperature measurements of the jovian planets and Titan from CCD-spectrophotometry. *Icarus* **133**, 134–146.

Kossacki, K. J., and R. D. Lorenz 1996. Hiding Titan's ocean: Densification and hydrocarbon storage in an icy regolith. *Planet. Space Sci.* **44**, 1029–1037.

Kuiper, G. P. 1944. Titan: A satellite with an atmosphere. *Astrophys. J.* **100**, 378–383.

Lellouch, E., A. Coustenis, D. Gautier, F. Raulin, N. Dubouloz, and C. Frère 1989. Titan's atmosphere and hypothesized ocean: A reanalysis of the Voyager 1 radiooccultation and IRIS 7.7-μm data. *Icarus* **79**, 328–349.

Lorenz, R. D. 1993. The life, death and afterlife of a raindrop on Titan. *Planet. Space Sci.* **41**, 647–655.

Lorenz, R. D. 1996. Pillow lava on Titan: Expectations and constraints on cryovolcanic processes. *Planet. Space Sci.* **44**, 1021–1028.

Lorenz, R. D., J. I. Lunine, P. G. Withers, and C. P. McKay 2001. Titan, Mars and Earth: Entropy production by latitudinal heat transport. *Geophys. Res. Lett.* **28**, 415–418.

Lorenz, R. D., C. P. McKay, and J. I. Lunine 1997. Photochemically driven collapse of Titan's atmosphere. *Science* **275**, 642–644.

Lorenz, R. D., C. P. McKay, and J. I. Lunine 1999. Analytic investigation of climate stability on Titan: sensitivity to volatile inventory. *Planet. Space Sci.* **47**, 1503–1515.

Loveday, J. S., R. J. Nelmes, M. Guthrie, S. A. Belmonte, D. R. Allan, D. D. Klug, J. S. Tse, and Y. P. Handa 2001. Stable methane hydrate above 2 GPa and the source of Titan's atmospheric methane. *Nature* **410**, 661–663.

Lunine, J. I., D. J. Stevenson, and Y. L. Yung 1983. Ethane ocean on Titan. *Science* **222**, 1229–1230.

McKay, C. P., A. Coustenis, R. E. Samuelson, M. T. Lemmon, R. D. Lorenz, M. Cabane, P. Rannou, and P. Drossart 2001. Physical properties of the organic aerosols and clouds on Titan. *Planet. Space Sci.* **49**, 79–99.

McKay, C. P., S. C. Martin, C. A. Griffith, and R. M. Keller 1997. Temperature lapse rate and methane in Titan's troposphere. *Icarus* **129**, 498–505.

McKay, C. P., J. B. Pollack, and R. Courtin 1989. The thermal structure of Titan's atmosphere. *Icarus* **80**, 23–53.

McKay, C. P., J. B. Pollack, J. I. Lunine and R. Courtin 1993. Coupled atmosphere–ocean models of Titan's past. *Icarus* **102**, 88–98.

Migeotte, M. V. 1948. Spectroscopic evidence of methane in the Earth's atmosphere. *Phys. Rev.* **7**, 519–520.

Moses, J. I., M. Allen, and Y. L. Yung 1992. Hydrocarbon nucleation and aerosol formation in Neptune's atmosphere. *Icarus* **99**, 318–346.

Peixoto, J. P., and A. H. Oort 1992. *Physics of Climate*. American Institute of Physics, New York.

Pruppacher, H. R., and J. D. Klett 1978. *Microphysics of Clouds and Precipitation*. D. Reidel, Dordrecht.

Samuelson, R. E., and L. A. Mayo 1997. Steady-state model for methane condensation in Titan's troposphere. *Planet. Space Sci.* **45**, 949–958.

Samuelson, R. E., N. R. Nath, and A. Borysow 1997. Gaseous abundances and methane supersaturation in Titan's troposphere. *Planet. Space Sci.* **45**, 959–980.

Schubert, G. 1983. General circulation and the dynamical state of the Venus atmosphere. In *Venus* (D. M. Hunten, L. Colin, T. M. Donahue, and V. I. Moroz, Eds.), pp. Univ. of Arizona Press, Tucson.

Stevenson, D. J., and B. E. Potter 1986. Titan's latitudinal temperature distribution and seasonal cycle. *Geophys. Res. Lett.* **13**, 93–96.

Suarez, M. J., and L. L. Takacs 1995. Documentation of the ARIES/GEOS dynamical core: Version 2. NASA Techn. Memorandum 104606, Vol. 5.

Takacs, L. L., A. Molod, and T. Wang 1994. Documentation of the Goddard Earth Observing System (GEOS) general circulation model–Version 1. NASA Techn. Memorandum 104606, Vol. 1.

Thompson, W. R., J. A. Zollweg, and D. H. Gabis 1992. Vapor-liquid equilibrium thermodynamics of $N_2 + CH_4$: Model and Titan applications. *Icarus* **97**, 187–199.

Tokano, T., F. M. Neubauer, M. Laube, and C. P. McKay 1999. Seasonal variation of Titan's atmospheric structure simulated by a general circulation model. *Planet. Space Sci.* **47**, 493–520.

Tokano, T., G. J. Molina-Cuberos, H. Lammer, and W. Stumptner 2001. Modelling of thunderclouds and lightning generation on Titan. *Planet. Space Sci.* **49**, 539–560.

Toon, O. B., C. P. McKay, R. Courtin, and T. P. Ackerman 1988. Methane rain on Titan. *Icarus* **75**, 255–284.

Yelle, R. V., D. F. Strobel, E. Lellouch, and D. Gautier 1997. Engineering models for Titan's atmosphere. In *Huygens: Science, Payload and Mission*, ESA SP-1177, pp. 243–256.

Yung, Y. L., M. Allen, and J. P. Pinto 1984. Photochemistry of the atmosphere of Titan: Comparison between model and observations. *Astrophys. J. Suppl. Ser.* **55**, 465–506.